# STRUCTRURAL BASIS OF TRANSCRIPTION INHIBITION BY THE NUCLEOSIDE-ANALOG INHIBITOR THURINGIENSIN

**By**

**RUIHENG YIN**

**A thesis submitted to the**

**Graduate School-New Brunswick**

**And**

**The Graduate School of Biomedical Sciences**

**Rutgers, The State University of New Jersey**

**In partial fulfillment of the requirements**

**For the degree of**

**Master of Science**

**Graduate Program in Biochemistry**

**Written under the direction of**

**Dr. Richard Ebright**

**And approved by**

_____

_____

_____

**New Brunswick, New Jersey**

**May, 2016**

**ABSTRACT OF THE THESIS**

**Structural Basis of Transcription Inhibition by**

**the Nucleoside-Analog Inhibitor Thuringiensin**

**by RUIHENG YIN**

**Thesis Director:**

**Dr. Richard Ebright**

Thuringiensin (Thg), also known as β-exotoxin, is an adenosine-containing secondary metabolite produced by the soil bacterium *Bacillus thuringiensis*. Thg exerts broad-spectrum bactericidal activity, insecticidal activity, and mammalian toxicity by inhibiting bacterial RNA polymerase (RNAP) and eukaryotic RNAP I, II, and III. Biochemical evidence indicates that Thg inhibits RNAP by functioning as a nucleoside-analog inhibitor (NAI) that competes with ATP for occupancy of the RNAP active center "i+1" nucleotide binding site.

We have determined a crystal structure of a *Thermus thermophilus* initial transcribing complex in

complex with Thg (RPo-GpA-Thg; resolution = 3.2 Å; $R_{free}$ = 25.4%). The structure shows that Thg occupies the RNAP active-center "i+1" nucleotide-binding site. The adenine and ribose moieties of Thg make the same interactions with a DNA template-strand thymine, the RNA 3'-nucleotide base, and the RNAP "i+1" NTP binding site as are made by the adenine and ribose moieties of ATP. The phosphate, allaric acid, and glucose moieties of Thg make interactions that mimic interactions made by the triphosphate moiety of ATP. In particular, the phosphate moiety of Thg occupies essentially the same position as is occupied by the γ-phosphate of ATP, and the phosphate moiety and one carboxy group of the allaric acid moiety of Thg coordinate a $Mg^{2+}$ ion ($Mg^{2+}$ II) in essentially the same manner and same position as the γ-phosphate and β-phosphate of ATP coordinate $Mg^{2+}$ II. The structure shows conclusively that Thg inhibits RNAP by functioning as an NAI that competes with ATP for binding to the RNAP active center "i+1" nucleotide binding site.

This structure of RNAP in complex with the non-selective NAI Thg is one of the first two structures of a bacterial RNAP in complex with an NAI. NAIs of viral nucleotide polymerases have been the subject of intense interest, and immense importance, for the development of anti-HIV and anti-HCV drugs. NAIs of bacterial RNAP only now are beginning to be explored, but show high promise for the development of antibacterial drugs. The structures of the RNAP-Thg complexes provide a starting point for structure-based understanding of bacterial-RNAP-selectivity of NAIs and for structure-based design of more potent bacterial-RNAP-selective NAIs.

## Acknowledgement

I would like to thank my thesis advisor Dr. Richard Ebright for his guidance and support during this research work. His enthusiasm about research, his decades of dedication to the field, and his creative, critical and thorough way of thinking have made a great impact on my life. I would also like to thank my committee members, Dr. Eddy Arnold and Dr. Wilma Olson for their review of this work. Dr. Eddy Arnold, the advisor of my third lab rotation, has provided valuable guidance in my crystallography studies.

In addition, I would like to thank the lab members in the Ebright lab. I really appreciate Yu Zhang, a previous postdoc in the lab, who helped me when I first started my research in crystallography and gave me much intelligent guidance for my research. I would like to thank Yu Feng, also an excellent crystallographer and a knowledgeable person, who is always patient with my questions and helped me in solving technique problems. I would like to thank David Degen, a postdoc in our lab, who generously provided advice for my thesis research on thuringiensin. I am thankful to Yon Ebright's guidance with the chemistry aspect of my research. Her diligence for her work has been a good role model for me. I also would like to thank Miaoxin Lin for her support and encouragement during my time in the lab. I would like to thank all the lab members for making the lab not only a place to work but also like a family for me.

Finally, I would like to thank my parents, my family and my beloved friends who have always been there for me and support me to overcome difficulties and make achievements.

# Table of Contents

## List of Tables



## List of Illustrations

# 1 Introduction

The rapid development of bacterial resistance across the world has made it a major public health issue and a worldwide crisis, endangering the existing effective antibiotics which have saved millions of lives (Ventola, 2015). There is an urgent need to develop new antibacterial agents that function through mechanisms that are different from current antibiotics for which bacterial resistance has developed, and thus that will be able to kill these resistant pathogens.

## 1.1 Bacterial RNAP

Bacterial RNA polymerase (RNAP) is a target for antibacterial therapy. The rationale for which bacterial RNAP is a suitable target for antibacterial therapy is: (1) RNAP is an essential enzyme necessary for the survival of living cells, providing efficacy for inhibitors targeting bacterial RNAP; (2) the sequences of bacterial RNAP subunits are highly conserved across bacteria species, allowing broad spectrum activity; (3) the sequence of bacterial RNAP is not highly conserved with that of eukaryotic RNAP, providing the potential for therapeutic selectivity for inhibitors specifically targeting bacteria (Chopra, 2007).

RNAP is the enzyme responsible for transcription and is one of the most regulated targets for transcription in the cell (Losick et al., 1976; Naryshkin et al., 2000). Bacterial RNAP is a large enzyme (~450 kD). Its core enzyme consists of one β subunit (~150 kD), one β' subunit (~160

kD), two identical α subunits (~35 kD), and one ω subunit (~10 Kd) (Naryshkin et al., 2000). The dimensions of the bacterial RNAP core enzyme is about 150Å × 115 Å ×100 Å and its shape mimics a crab claw (Naryshkin et al., 2000). As shown in Figure 1, the β and β' subunits form the two "pincers" of the claw, and there are extensive interactions between them (Zhang et al., 1999). The two "pincers" form an active center cleft with a diameter of ~25 Å. This is a suitable size to accommodate DNA in its double stranded form, whose entry into the active center cleft and unwinding is necessary for transcription to occur (Naryshkin et al., 2000). The two α subunits are located distal to the active center. $\alpha^{I}$ primarily binds to the β subunit and $\alpha^{II}$ primarily binds to the β' subunit. The ω subunit is located distal to the active center, at the base of β' pincer. It is not essential for the function of RNAP, but is believed to help stabilize the complex (Minakhin et al., 2001).

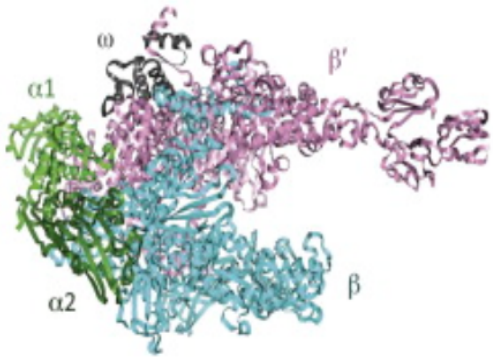


**Figure 1. *Thermus aquaticus* RNAP core enzyme structure**
(Zhang et al., 1999)

While the bacterial RNAP core enzyme is able to perform non-specific transcription, independent of promoter, it needs to recruit another subunit (σ subunit) to have the ability to conduct promoter-dependent, sequence specific transcription, resulting in a bacterial RNAP holoenzyme (Burgess et al., 1969). The σ subunit is responsible for recognition of specific promoters

(deHaseth et al., 1998) and facilitates promoter unwinding during transcription initiation (Zhang et al., 2012).

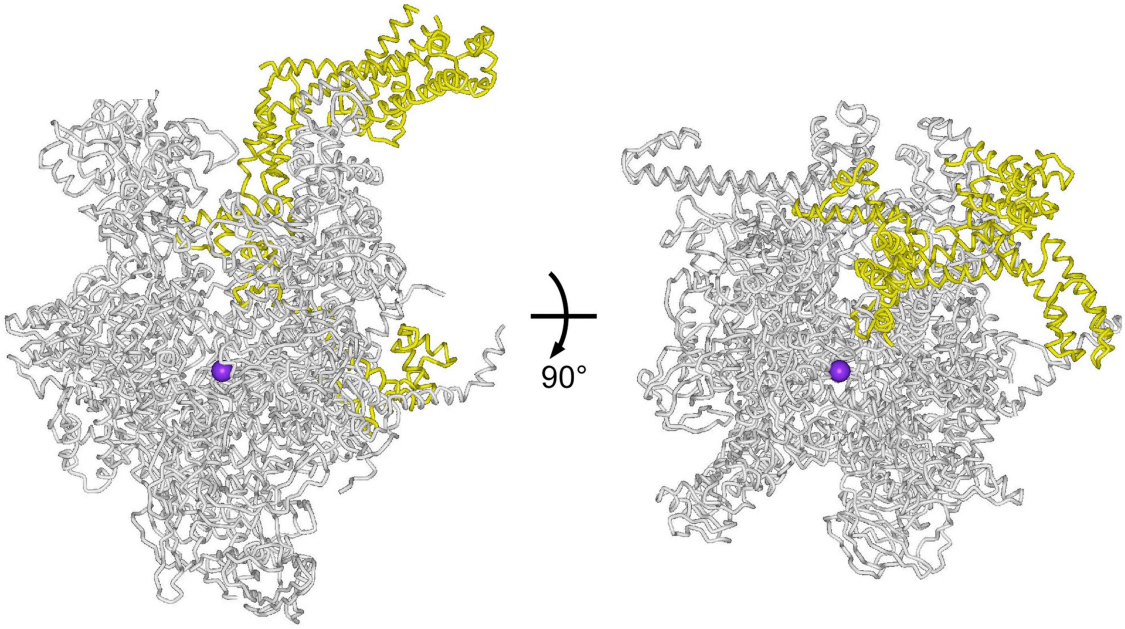


**Figure 2. *Escherichia coli* RNAP holoenzyme structure (two orthogonal views)**
RNAP core is in gray; *E.coli* $\sigma^{70}$ is in yellow; active center $Mg^{2+}$ (I) is in purple sphere (Degen et al., 2014)

RNAP performs transcription by synthesizing RNA from a DNA template. There are three main steps in transcription: initiation, elongation and termination (Figure 3) (Saecker et al., 2011). During promoter-dependent transcription initiation, the RNAP holoenzyme first binds to promoter DNA and forms the RNAP promoter closed complex (RPc). Then double-stranded DNA is inserted into the active center cleft and is melted to form a ~12 nucleotide transcription bubble in single-stranded form, which is the RNAP promoter open complex (RPo) (Zhang et al., 2012). Once the transcription process begins, the enzyme transitions to become the initial transcribing

complex (RPitc). After several cycles of abortive RNA synthesis following the formation of RPitc, RNAP will finally escape the promoter and enter into the transcription elongation stage (Kapanidis et al., 2006; Revyakin et al., 2006).

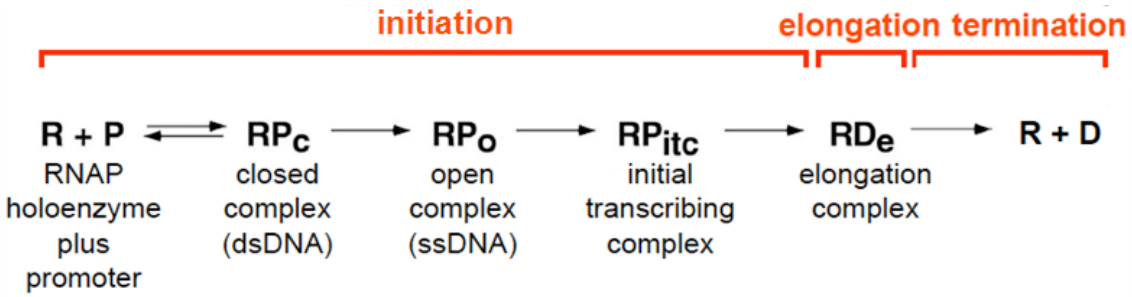


**Figure 3. Schematic of transcription process**

### 1.2 RNAP active center

The region of major interaction between the β and β' subunits occurs at the base of active-center cleft, the location of the bacterial RNAP active center (Zhang et al., 1999). The RNAP active center is the engine of the molecule, which has robost organization, yet is sensitive to regulation, and controls the processivity and fidelity of transcription (Nudler, 2009). The active center $Mg^{2+}$ (I) ion is coordinated by three conserved aspartic acids of an absolutely conserved motif of the β' subunit: -NADFDGD- (Zhang et al., 1999), which is shown in Figure 4A, B. The primary RNAP enzymatic activity is to transfer a nucleotidyl moiety from the incoming NTP to the 3'-end hydroxyl of a newly synthesized RNA strand (Sosunov et al., 2003). The site in the active center where the newly synthesized RNA 3'-end is located is called the "i" site. This is also the binding

site of first initiating nucleotide during the initial RNA synthesis. The site for the binding of the extending nucleotide is named the "i+1" site (Sosunov et al., 2003). A phosphodiester bond forms between the 3'-end hydroxyl of RNA and the α phosphate of the incoming NTP, followed by the new 3'-end RNA translocating from the "i+1" site to the "i" site and releasing the pyrophosphate

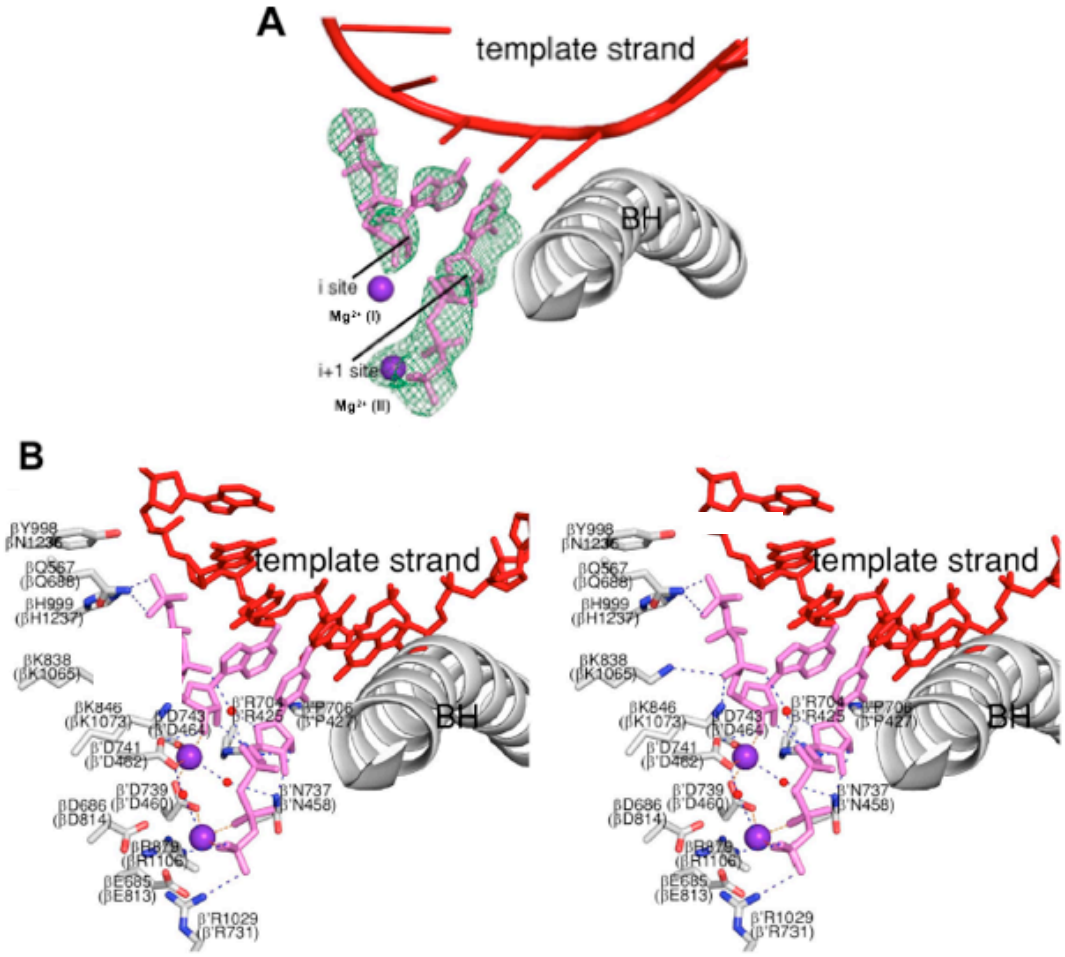


**Figure 4. Structure of *T.thermophilus* RPo-ATP-CMPcPP**

(Zhang et al., 2014)

(A) Structure showing the active center "i" site and "i+1" site. Pink sticks, ATP and CMPcPP. Purple spheres, $Mg^{2+}$ (I) and $Mg^{2+}$ (II).

(B) Interactions at the active center. Residues are numbered as in *T.thermophilus* RNAP and *E.coli* RNAP in the parentheses.

(PPi) (Nudler, 2009). The second $Mg^{2+}$ (II) is carried in by the incoming NTP (Figure 4) and is released with PPi product (Da et al., 2013). The two $Mg^{2+}$ ions have important catalytic activity and are responsible for phosphodiester bond formation (Sosunov et al., 2003).

### 1.3 RNAP active-center-directed inhibitors

Discovering and studying RNAP active-center-directed inhibitors is an attractive subject because the target at the active-center is different from the targets of previously characterized bacterial RNAP inhibitors and provides a promising site for developing new effective antibactrial drugs (Zhang et al., 2014).

#### 1.3.1 Non-nucleoside-analog inhibitor: GE23077

Researchers identified a non-nucleoside-analog inhibitor, GE23077, which, for the first time, directly targets the bacterial RNAP active center and prevents transcription initiation (Zhang et al., 2014). GE23077 is produced by the soil bacterium *Actinomadura sp.* DSMZ 13491 and is a cyclic-peptide antibiotic (Figure 5) (Ciciliato et al., 2004).

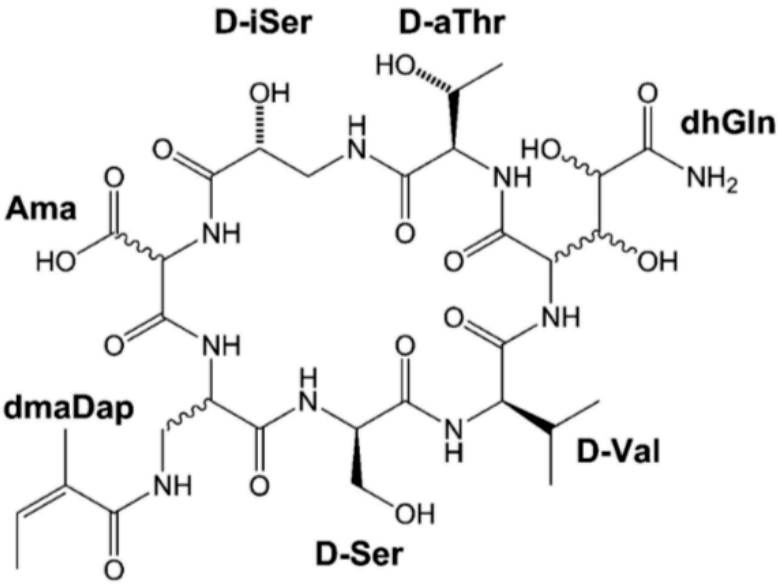


**Figure 5. Chemical structure of GE23077**

(Zhang et al., 2014)

GE23077 specifically inhibits transcription initiation and not tanscription elongation. It prevents the binding of the first initiating nucleotide needed for RNA synthesis (Zhang et al., 2014). The target of GE23077 is different from previous identified RNAP inhibitors, such as sorangicin (Sor) (Campbell et al., 2005), myxopyronin (Myx), corallopyronin (Cor), ripostatin (Rip), lipiarmycin (Lpm), streptolydigin (Stl) (Ho et al., 2009), CBR703 (CBR) (Artsimovitch et al., 2003), and microcin J25 (MccJ25) (Mukhopadhyay et al., 2004). The resistance determinant for GE23077 is significantly smaller than that of other RNAP inhibitors, which is not surprising because the binding site of GE23077 includes essential amino acids in the RNAP active center which cannot be substituted without loss of RNAP enzymetic activity (Zhang et al., 2014).

GE23077 inhibits transcription initiation not by inhibiting the formation of RPo, but rather by inhibiting the following steps during the first nucleotide addition (Zhang et al., 2014). GE23077 directly binds to the RNAP active center core catalytic components: the "i" site, the "i+1" site and directly interacts with $Mg^{2+}$ (I) (Figure 6) (Zhang et al., 2014). There is a mutually exclusive binding machanism between GE and initiating nuceotides (Figure 6). When GE first binds to RNAP and occupies the "i" site and the "i+1" site at the active center, initiating nuceotides can no longer bind at the same location, as is necessary for initiating RNA synthesis (Zhang et al., 2014).

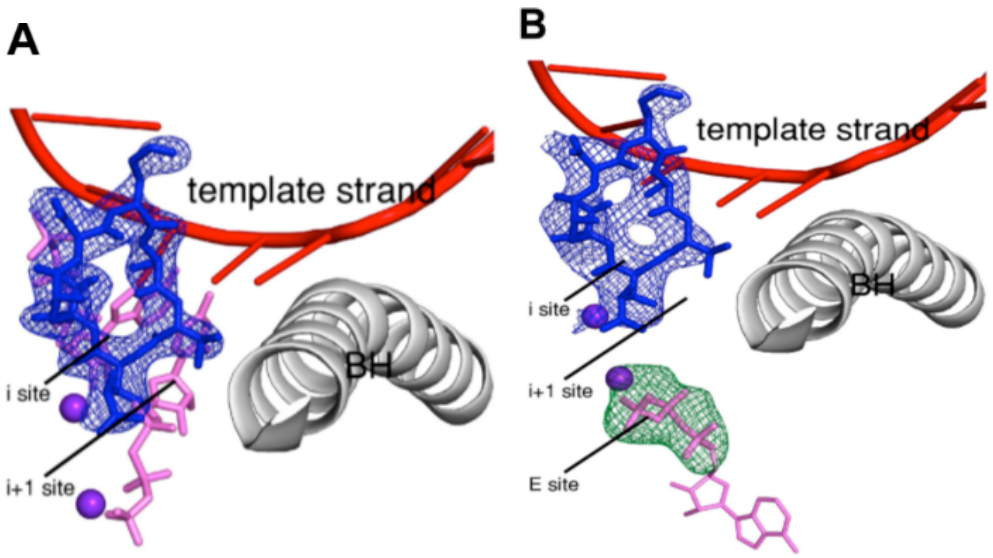


**Figure 6. Mutually exclusive binding between GE and initiating NTPs**
(Zhang et al., 2014)

(A) Superimposition of *T.thermophilus* RPo-GE and RPo-ATP-CMPcPP structures at the active center "i" site and "i+1" site. Pink sticks, ATP and CMPcPP. Blue stick, GE. Bule mesh, electron density for GE. Purple spheres, $Mg^{2+}$ (I) and $Mg^{2+}$ (II).
(B) Structure of RPo first soaked with GE then soaked with ATP and CMPcPP.

### 1.3.2 Nucleoside-analog inhibitor (NAI): thuringiensin

Another class of RNAP active-center-directed inhibitor is the nucleoside-analog inhibitor (NAI). Thuringiensin (Thg), also known as β-exotoxin, is a thermostable, secondary metabolite from the soil bacterium *Bacillus thuringiensis* (Liu et al., 2014). Biochemical evidence has shown that it is an NAI (Sebesta et al., 1969). Its chemical formula is C22H32O19N5P and its chemical structure is shown in Figure 7. Thg is composed of adenosine, glucose, phosphate and allaric acid.

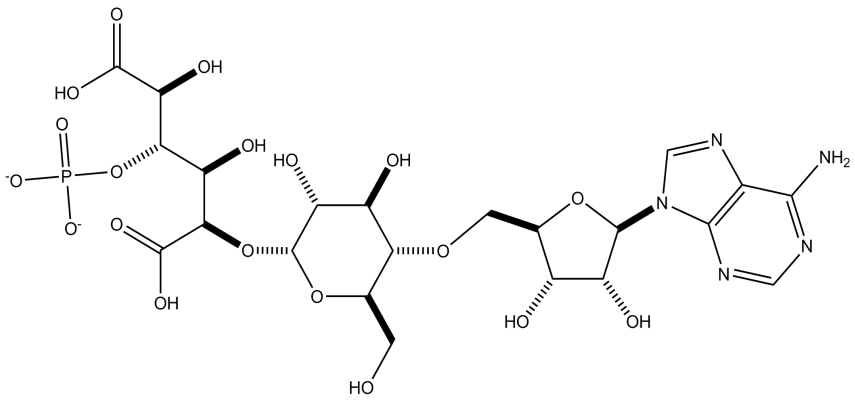

**Figure 7. Chemical structure of Thuringiensin**

Thg has broad spectrum bactericidal activity, insecticidal activity, and mammalian toxicity by inhibiting both bacterial RNA polymerase (RNAP) and eukaryotic RNAP I, II, and III (Kireeva et al., 2012; Liu et al., 2014; Seibold et al., 2010).

Researchers have performed experiments to study the mechanism of RNAP inhibition by Thg

both *in vivo* and *in vitro* (Kireeva et al., 2012). Thg inhibits both the initiation and elongation stages of RNA synthesis (Sebesta et al., 1969). All evidence indicated that inhibition of RNAP by Thg can be overcome by ATP (Kireeva et al., 2012). The competitive behavior suggests that Thg and ATP bind to the same site on RNAP. The adenosine moiety of Thg resembles the adenosine of ATP and phosphorylated allaric acid mimics the triphosphate component of ATP.

The function of the individual parts of Thg has also been studied. Substituting the base, adenosine, of Thg with inosine maintained the inhibitory activity of Thg, but now the inhibition could only be reversed by GTP rather than ATP (Sebesta and Horska, 1970). The phosphoric acid and allaric acid group of Thg are also required for RNAP inhibition, but their exact role was ambiguous (Farkas et al., 1969).

In conclusion, biochemical evidence indicates that Thg inhibits RNAP by functioning as a nucleoside-analog inhibitor (NAI) that competes with ATP for occupancy of the RNAP active-center nucleotide binding site. Here we have obtained a high resolution structure of Thg in complex with RPo-GpA which provides the structural basis for transcription inhibition by Thg.

# 2 Material and Methods

## 2.1 *T.thermophilus* RNA polymerase purification

### 2.1.1 *T.thermophilus* RNAP core enzyme

*T. thermophilus* strain HB-8 (DSM579; Deutsche Sammlung von Mikroorganismen und Zellkulturen GmbH) was used to isolate *T.thermophilus* RNAP core enzyme. The method used to isolate *T.thermophilus* RNAP core is described in (Vassylyeva et al., 2002), but the step of gel-filtration chromatography on Superdex S200HR was omitted. After concentrating to ~10 mg/ml using 30 kDa MWCO Amicon Ultra-15 centrifugal ultrafilters (Millipore, Inc.), samples were stored in 1 mM EDTA, 150 mM NaCl, 20 mM Tris-HCl, pH 7.9, 5% glycerol and 1 mM dithiothreitol at -80°C. The yields were 0.5 mg/L, and purities were >95%.

### 2.1.2 *T.thermophilus* RNAP holoenzyme

*T. thermophilus* $\sigma^A$ was purified as in (Zhang et al., 2012). A mixture of *T. thermophilus* RNAP core (13 μM) and *T. thermophilus* $\sigma^A$ (52 μM) were incubated in 2 ml 150 mM NaCl, 20 mM Tris-HCl, pH 7.7, and 2% glycerol for 12 h at 4°C. Then the mixture was applied to a HiLoad 16/60 Superdex S200 column (GE Healthcare, Inc.) equilibrated with 100 mM NaCl, 20 mM Tris-HCl, pH 7.7, and 1% glycerol. The protein was eluted with 180 ml of the same buffer. Fractions containing *T. thermophilus* RNAP holoenzyme were collected (usually between 47 and 57 ml of elution volume). After concentrating to ~7.5 mg/ml using 30 kDa MWCO Amicon Ultra-15 centrifugal ultrafilters (Millipore, Inc.), samples were stored at -80°C in the same buffer.

### 2.2 Thuringiensin preparation

Thuringiensin was obtained from a lab in France and had poor purity. Thg was purified using a 6cc (1 g) Sep-Pak C18 cartridge, and eluting with 30%, 60% and 100% acetonitrile. To determine its purity, after drying by vacuum, the material was weighted, redissolved in water, and the concentration of Thg was determined by UV absorbance at wavelength 260nm. Dried Thg was stored at -20°C.

### 2.3 RNAP-inhibitory activity: ribogreen transcription assay

Ribogreen fluorescence-detected transcription assays were performed to determine the half-maximal inhibitory concentrations (IC50) of Thg against bacterial RNAP (Srivastava et al., 2011). 20 µl reaction mixtures contained 0-125 µM Thg (in water), bacterial RNAP holoenzyme (75 nM E. coli RNAP holoenzyme or 75 nM *T.thermophilus* RNAP holoenzyme), 20 nM DNA fragment carrying the bacteriophage T4 N25 promoter, ATP, GTP, UTP, and CTP (all at 100 µM concentration) in 10 mM MgCl2, 100 mM KCl, 50 mM Tris-HCl, pH 8.0, 1 mM DTT, 10 µg/ml bovine serum albumin, 5.5% glycerol. Reaction mixtures except DNA and NTPs were pre-incubated for 10 min at 37°C. DNA was then added and incubated for 15 min at 37°C, followed by the addition of NTPs and incubation for 60 min at 37°C. The template DNA was then digested by the adding 1 µl 5 mM CaCl2 and 2 U DNaseI (Ambion) and incubating for 90 min at 37°C. RNA was quantified by adding 100 µl 1:500 diluted Quant-iT RiboGreen RNA Reagent (Life Technologies) in 1 mM EDTA and 10 mM Tris-HCl, pH 8.0, incubating at 22°C for 10 min, and measuring fluorescence intensity using a 485 nm excitation wavelength and a 535 nm emission

wavelength (GENios Pro microplate reader (Tecan)). Data was plotted in SigmaPlot 8.0 (SPSS) and the IC50 value was calculated by non-linear regression.

### 2.4 Nucleic-acid scaffold construction

The nucleic-acid scaffold used for the formation of RPo-GpA complex is shown in Figure 8 below. It is consisted of one DNA nontemplate strand, one DNA template strand, and a ribodinucleotide, GpA, which is complementary to the -1 and +1 positions of the DNA template strand. The nontemplate and template strands are complementary to each other from the +3 position towards the downstream. The upstream of the nontemplate strand contains a -10 element and a discriminator element which have specific interactions with the RNAP holoenzyme.

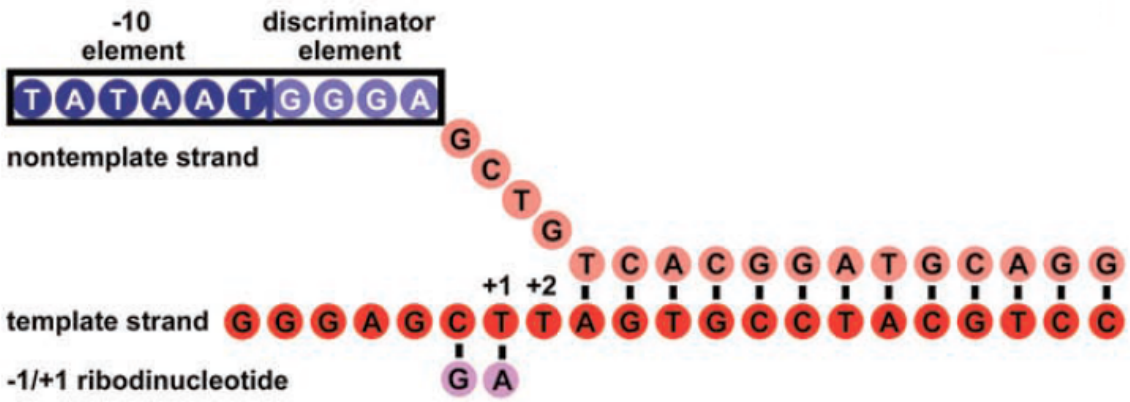


**Figure 8. Nucleic-acid scaffold for RPo-GpA complex formation**

The scaffold is essentially the same as in the paper (Zhang et al., 2012) except that the G at +2 positon of template strand is changed to a T. The upper DNA strand shows the sequence of the nontemplate strand and the lower DNA strand in red color shows the sequence of the template strand. The ribodinucleotide GpA complementary to -1 and +1 positions of the template strand is shown in purple. The scaffold is double stranded starting at +3 position to downstream, while the rest of the scaffold forms part of the transcription bubble.

Prior to nucleic-acid scaffold preparation, 3mM oligodeoxyribonucleotides (IDT, Inc.) and 25mM ribodinucleotide GpA (RiboMed, Inc) were dissolved using ultrapure nuclease free water (GIBCO, Inc.) and stored at -80°C. A 25ul mixture containing 0.55mM template strand oligodeoxyribonucleotide, 0.5mM nontemplate-strand oligodeoxyribonucleotide, pH 7.7, 200mM NaCl, 10mM $MgCl_2$ and 5mM Tris-HCl was quickly heated to, and keep at, 95°C for 5min. The mixture was then slowly cooled at a rate of 2°C per min until reaching 25°C. This process is controlled by a thermal cycler (Applied Biosystems, Inc.). The prepared scaffold mixture was stored at -80°C.

### 2.5 Structure determination

#### 2.5.1 Formation of RNAP-promoter open complex

The procedure for RNAP-promoter open complex formation follows the paper (Zhang et al., 2012). The RPo-GpA complexes for crystallization were prepared by mixing 20 µl 10 µM *T.thermophilus* holoenzyme (in buffer containing 100 mM NaCl, 20 mM Tris-HCl, pH 7.7, and 1% glycerol), 1 µl 0.5 mM of the nucleic-acid scaffold (in 200 mM NaCl, 10 mM MgCl2 and 5 mM Tris-HCl, pH 7.7), and 1 µl 25 mM ribodinucleotide GpA (in water). The mixture was incubated at room temperature (22°C) for 1h, resulting in RPo-GpA complex.

#### 2.5.2 Crystallization

The hanging-drop vapor-diffusion technique was used for crystallization. The optimized conditions for crystallization of RPo-GpA are as follows: the drop contains 1 µl 18 µM RPo-GpA

complex (in 100 mM NaCl, 20 mM Tris-HCl, pH 7.7, and 1% glycerol) plus 1 µl reservoir solution; the reservoir contains 200 mM KCl, 50 mM MgCl2, 400 µl 100 mM Tris-HCl, pH 8.7 and 10% PEG4000; the temperature for crystal growth is 22°C (Zhang et al., 2012). These conditions yielded rod-like crystals in one day. These crystals were then used as micro-seeds under the same conditions. High quality crystals appeared within one week with dimensions of 0.3 mm x 0.1 mm x 0.1 mm.

#### 2.5.3 Inhibitor soaking and cryo-cooling

Thg was soaked into RPo-GpA crystals by addition of 0.2 µl 20 mM Thg (dissolved in reservoir solution) to the hanging drop, and incubation at 22°C for 15 min. Crystals were transferred stepwise to reservoir solutions containing 1 mM Thg and 0.5%, 1%, 2.5%, 5%, 10%, 14% and 17.5% (2R, 3R)-(-)-2,3-butanediol (Sigma-Aldrich, Inc.). Crystals were in the first step for 30s, and 2s each for the remaining steps. The crystals were then flash-cooled with liquid nitrogen.

#### 2.5.4 Data collection and reduction

The diffraction data of the above cryo-cooled crystals were collected at the F1 beamline, Cornell High Energy Synchrotron Source (CHESS). Data was processed by HKL2000 (Vassylyev et al., 2007a) at CHESS.

#### 2.5.5 Structure solution and refinement

French-Wilson data correction in Phenix was used to convert structure factors (Vassylyev et al.,

2007b). Anisotropy correction was performed using the Diffraction Anisotropy server of UCLA-DOE LAB (Brotz-Oesterhelt and Brunner, 2008). Molecular replacement was used to solved the structure by Molrep (Vagin and Teplyakov, 1997) using one molecule from the structure of *T.thermophilus* RPo (PDB 4G7H) (Zhang et al., 2012) as the search model. The refinement strategies were as follows: (1) rigid-body refinement of the RNAP molecule; (2) rigid-body refinement by chain; (3) repetitive model building with Coot and refinement with Phenix (Adams et al., 2010; Emsley et al., 2010). Finally the DNA nontemplate strand, the DNA template strand, and Thg atomic models were built into mFo-DFc maps, and followed by repetitive model building and refinement. The refinement statistics are shown in the Results section.

## 3 Results

### 3.1 Thg inhibits transcription of *T.thermophilus* and *E.coli* RNAP

The results of ribogreen transcription assays (Figure 9) show that Thg inhibits the transcription activity of both *T.thermophilus* and *E.coli* RNAP *in vitro***.** Thg inhibits *E.coli* RNAP better than *T.thermophilus* RNAP. The IC50 value for *E.coli* RNAP is 3.89 μM, while the IC50 value for *T.thermophilus* RNAP is 49.00 μM. This indicates that *E.coli* RNAP may have different features at the active center that provide a higher affinity for Thg than *T.thermophilus* RNAP.

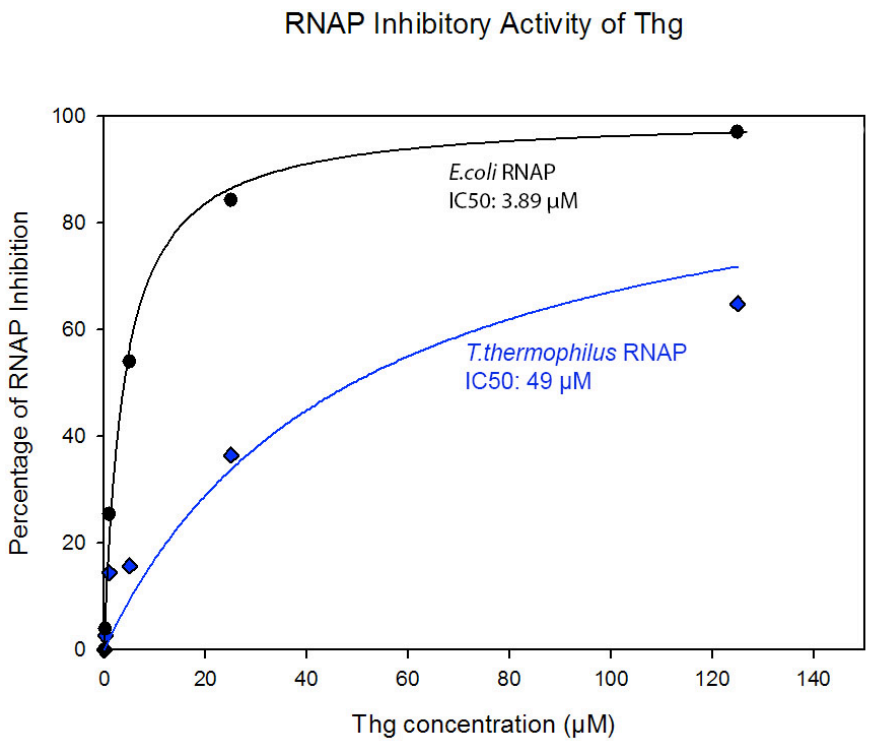


**Figure 9. RNAP inhibitory activity of Thg**

Result of ribogreen transcription assay. Percentage of RNAP inhibition (%) v.s. Thg concentration (μM) is plotted. IC50 values are labeled accordingly.

### 3.2 Crystal structure of *T. thermophilus* initial transcribing complex in complex with Thg

The crystal structure of a *T. thermophilus* initial transcribing complex in complex with Thg was determined at a resolution of 3.20 Å. This protein, nucleic acid, and inhibitor complex is comprised of *T. thermophilus* RNAP, $\sigma^A$, a nucleic acid scaffold (Figure 8) containing partial transcription bubble with promoter DNA fragment, double-stranded downstream DNA, a ribodinucleotide primer (GpA), and Thg. The structure is thus named RPo-GpA-Thg. The RPo-GpA-Thg crystals were obtained by soaking Thg into existing RPo-GpA crystals. The

crystallographic data and refinement statistics are shown in Table 1. The space group of the structure is C121 and the cell parameters are : a=185.3Å, b=103.0 Å, c=295.9 Å; α=90.0°, β=98.9°, γ=90.0°. This dataset reaches 100% completeness. The $R_{work}$ and Rfree are 0.211 and 0.254, respectively.

| | |
|---|---|
| dataset | Tth RPo-GpA-Thg |
| beamline | CHESS-F1 |
| space group | *C 121* |
| resolution range (Å) | 50.00-3.20 (3.26-3.20) |
| cell parameters (Å) | a=185.3, b=103.0, c=295.9<br>α=90.0°, β=98.9°, γ=90.0° |
| completeness | 1.000 (1.000) |
| multiplicity | 3.8 (3.6) |
| mean I/σ | 9.9 (1.5) |
| $R_{merge}$ | 0.127 (0.861) |
| $R_{work}/R_{free}$ | 0.211/0.254 |
| B factor (Å$^2$) | 54.6 |
| bond-length RMSD (Å) | 0.004 |
| bond-angle RMSD | 0.750° |

**Table 1. Crystallographic data and refinement statistics**

### 3.3 Thg binds to RNAP active center "i+1" site

The structure shows that Thg binds to the RNAP active-center region (Figure 10), in close proximity to the active-center $Mg^{2+}$ (I), which is consistent with the implications of the previous biochemical evidence. To be more specific, the structure shows that Thg binds to the RNAP active-center "i+1" site (Figure 11. C, D).

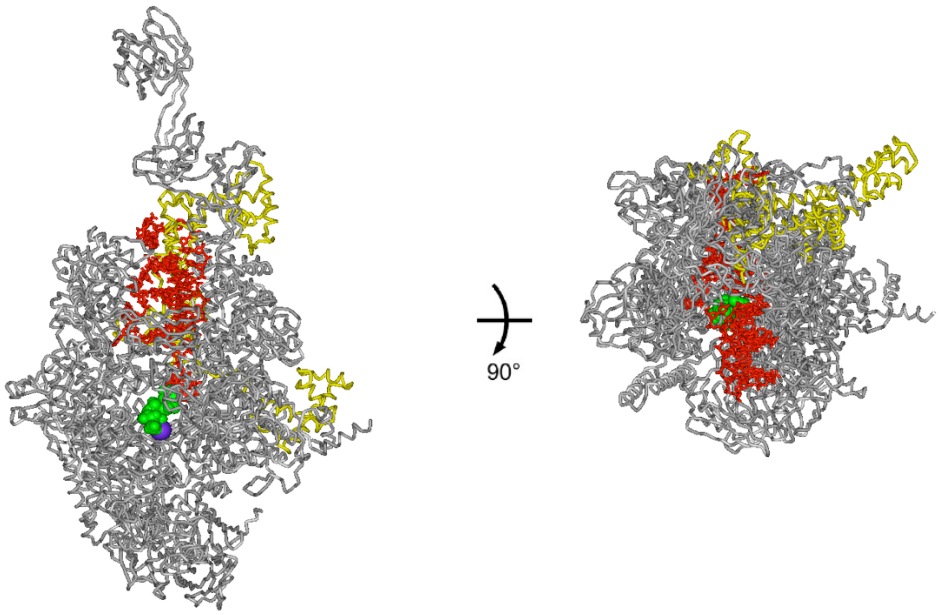


**Figure 10. Thg binds to the active center of RPo-GpA**

Overall crystal structure of RPo-GpA-Thg (two orthogonal views). Yellow color represents σ subunit; gray color represents the other subunits of RNAP; red color represents nucleic acid; green color represents Thg; purple sphere represents the active center $Mg^{2+}$ (I).

Previously, a crystal structure of RPo-GpA-CMPcPP was solved at 3.35 Å resolution (unpublished data) (Figure 11. A, B), showing the structure of RPo-GpA in complex with CMPcPP rather than Thg. CMPcPP is a non-reactive analog of CTP, with its oxygen connecting the α-phosphate and β-phosphate replaced with carbon. In this structure, CMPcPP binds to the active-center "i+1" site. By comparing the structures of RPo-GpA-CMPcPP (Figure 11. B) and RPo-GpA-Thg (Figure 11. C), we find that Thg occupies the same position, the active-center "i+1" site, as CMPcPP with unambiguous electron-density. Both CMPcPP and Thg coordinate

**A**

| | |
|---|---|
| dataset | Tth RPo-GpA-CMPcPP |
| beamline | CHESS-F1 |
| space group | *C*2 |
| resolution range (Å) | 50.00-3.35 (3.41-3.35) |
| cell parameters (Å) | a=183.4, b=104.3, c=297.3<br>α=90.0°, β=98.4°, γ=90.0° |
| completeness | 0.956 (0.891) |
| multiplicity | 5.3 (5.3) |
| mean I/σ | 7.7(1.8) |
| $R_{merge}$ | 0.197 (>1) |
| $R_{work}/R_{free}$ | 0.196/0.246 |
| B factor (Å$^2$) | 57.8 |
| bond-length RMSD (Å) | 0.007 |
| bond-angle RMSD | 0.727° |

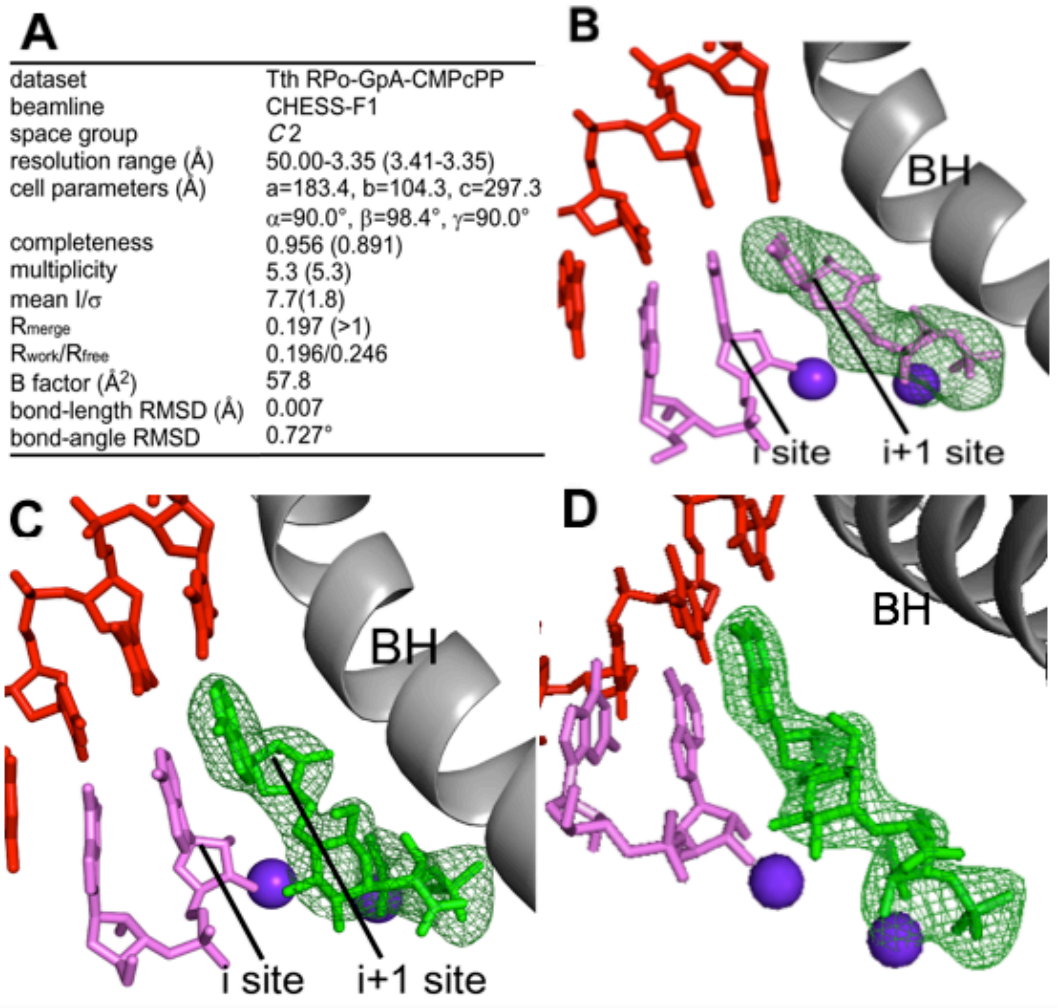


**Figure 11. Thg binds to the RNAP active center "i+1" site**

(A) Crystallographic data and refinement statistics of RPo-GpA-CMPcPP

(B) Crystal structure of RPo-GpA-CMPcPP: electron density and atomic model. Green mesh, mFo-DFc omit map for CMPcPP (contoured at 2.5σ); pink sticks, GpA and CMPcPP; red ribbon, DNA template strand; gray ribbon, RNAP bridge helix; purple spheres, $Mg^{2+}$ (I) and $Mg^{2+}$ (II).

(C) Crystal structure of RPo-GpA-Thg: electron density and atomic model. Green mesh, mFo-DFc omit map for Thg (contoured at 2.5σ); pink sticks, GpA; green sticks, Thg.

(D) Same as (C) but in a different view orientation.

$Mg^{2+}$ (II). The fact that Thg binds to the RNAP active center at the same position as CMPcPP further validates that Thg inhibits RNAP activity by functioning as an NAI. While CMPcPP pairs with G on the template strand, Thg, being an ATP analog, pairs with T on the template strand shown in the structures.

### 3.4 Thg binds to RNAP initial transcribing complex in a pre-insertion mode

There are two important subregions near the active center: the "trigger loop" (TL) and the "bridge helix" (BH). The TL changes its conformation (open/close) and the BH also changes its conformation (bent/unbent) during each nucleotide addition cycle (Degen et al., 2014). These conformational changes are important for nucleotide addition. The TL and BH help to dehydrate the active center (thus providing a favorable environment for catalysis), they place the extending nucleotide in close proximity to the RNA 3'-end hydroxyl (promoting bond formation), and they proofread if the extending nucleotide is correct (Kireeva et al., 2012; Seibold et al., 2010). The extending nucleotide can bind at the active center "i+1" site in either pre-insertion mode or insertion mode (Vassylyev et al., 2007b). In the insertion binding mode, the base of the incoming NTP is paired with the corresponding base on the DNA template strand, and stacked with the base of the RNA 3'-end. Its sugar and triphosphate moieties are also properly oriented and are ready for catalysis. The active center is dehydrated and the TL is in the closed conformation (Vassylyev et al., 2007b). In our structure of RPo-GpA-Thg, the TL is in an open conformation (Figure 12). The base of Thg is base-paired to the thymine in the DNA template strand and stacked with the

RNA base at the "i" site. However, its allaric acid and phosphate moieties are not properly oriented and cannot be catalyzed for bond formation at this binding mode. Thus we conclude that Thg binds to RPitc in a pre-insertion mode in our RPo-GpA-Thg structure.

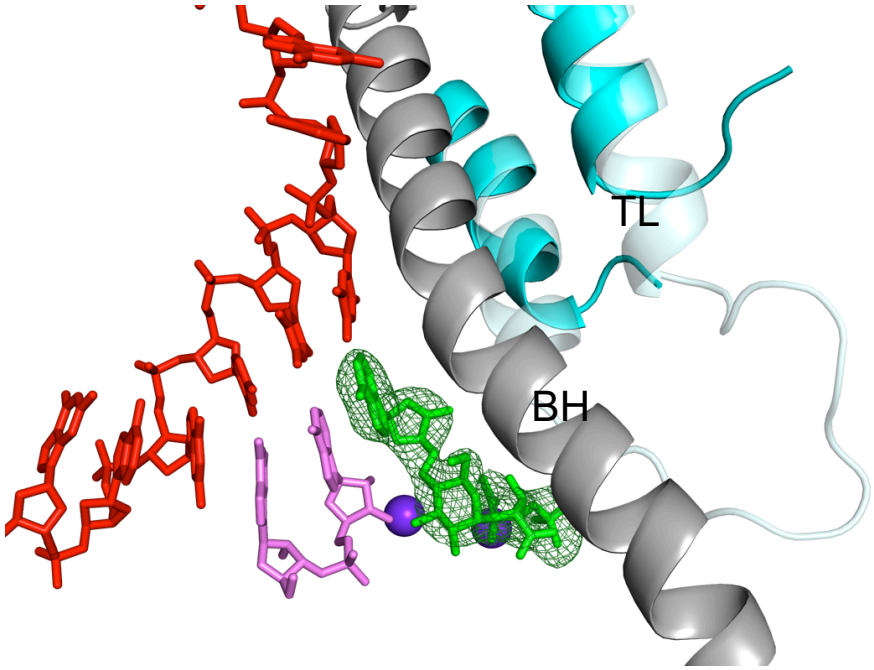


**Figure 12. Trigger loop is in open conformation in RPo-GpA-Thg**

Structure of RPo-GpA-Thg that shows the TL in an open conformation (cyan colored helix; the loop is missing because it is disordered when in the open conformation). The transparent, light-blue colored helix and loop represent the closed-form TL for comparison (from structure of RPo-GpA-CMPcPP). Red sticks, DNA template strand. Pink sticks, GpA. Green sticks, Thg. Purple spheres, $Mg^{2+}$ (I) and $Mg^{2+}$ (II).

### 3.5 Interactions between Thg and RNAP initial transcribing complex

Thg interacts with the RNAP initial transcribing complex (RPitc) at the active-center "i+1" site in the same way as CMPcPP (Figure 13, Figure 14). We can generalize the interaction patterns of

NTPs with RPitc at the “i+1” site from the structure of RPo-GpA-CMPcPP. ATP would have the same interactions with RPitc except that it base pairs with thymine instead of guanine. From the structure of RPo-GpA-Thg, we can conclude that the adenine and ribose moieties of Thg make the same interactions with a DNA template-strand thymine, the RNA 3’-nucleotide base, and the RNAP "i+1" NTP binding site as would be made by the adenine and ribose moieties of ATP. Specifically, the adenine moiety of Thg forms two hydrogen bonds with the DNA template-strand thymine and is stacked with the RNA 3’-nucleotide base in the “i” site. The hydroxyl of the ribose moiety of both Thg and CMPcPP form hydrogen bonds with residues β'Arg704 and β'Asn737 (Figure 13, Figure 14). The phosphate, allaric acid, and glucose moieties of Thg make interactions that mimic the interactions made by the triphosphate moiety of ATP. In particular, the phosphate moiety of Thg occupies essentially the same position as is occupied by the γ-phosphate of ATP. Both the phosphate of Thg and the γ-phosphate of CMPcPP form salt bridges with residues βArg879 and β'Arg1029 (Figure 13, Figure 14). The phosphate moiety and one carboxyl group of the allaric acid moiety of Thg coordinate a $Mg^{2+}$ ion ($Mg^{2+}$ II) in essentially the same manner and same position as the γ-phosphate and β-phosphate of an NTP coordinate $Mg^{2+}$ (II). Thg and CMPcPP also both have van der Waals interactions with β'Pro706, β'Asp739 and β'Asp741.

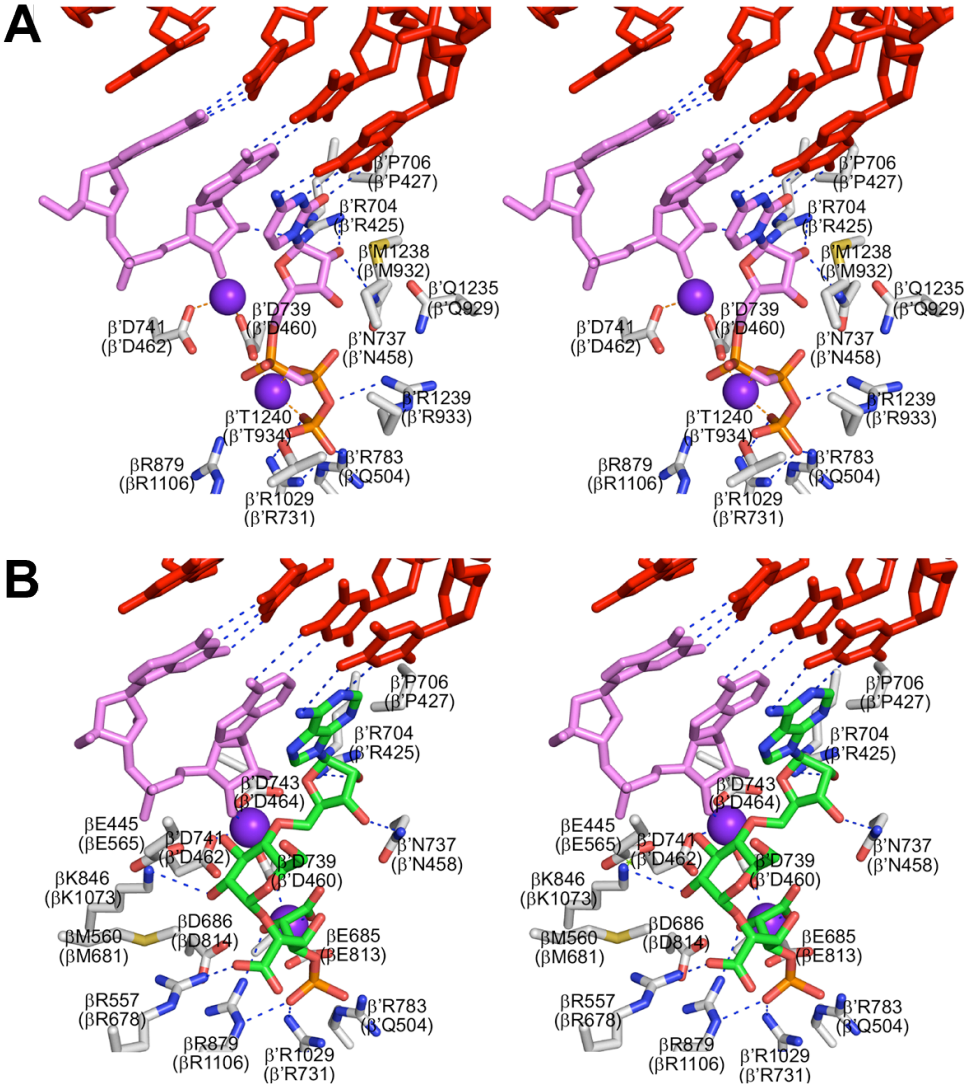


**Figure 13. Contacts between RNAP and CMPcPP/Thg (stereodiagram)**

(A) Structure of RPo-GpA-CMPcPP that shows interaction of CMPcPP with DNA template strand, GpA and RNAP residues. Red sticks, DNA template strand. Pink sticks, GpA and CMPcPP. White sticks, RNAP residues with labels numbered as in *T.thermophilus* RNAP and *E.coli* RNAP in the parentheses. Purple spheres, $Mg^{2+}$ (I) and $Mg^{2+}$ (II). Blue dashed lines, hydrogen bonds. Red dashed lines, bonds coordinating $Mg^{2+}$.

(B) Structure of RPo-GpA-Thg that shows interaction of Thg with DNA template strand, GpA and RNAP residues. Pink sticks, GpA. Green sticks, Thg.

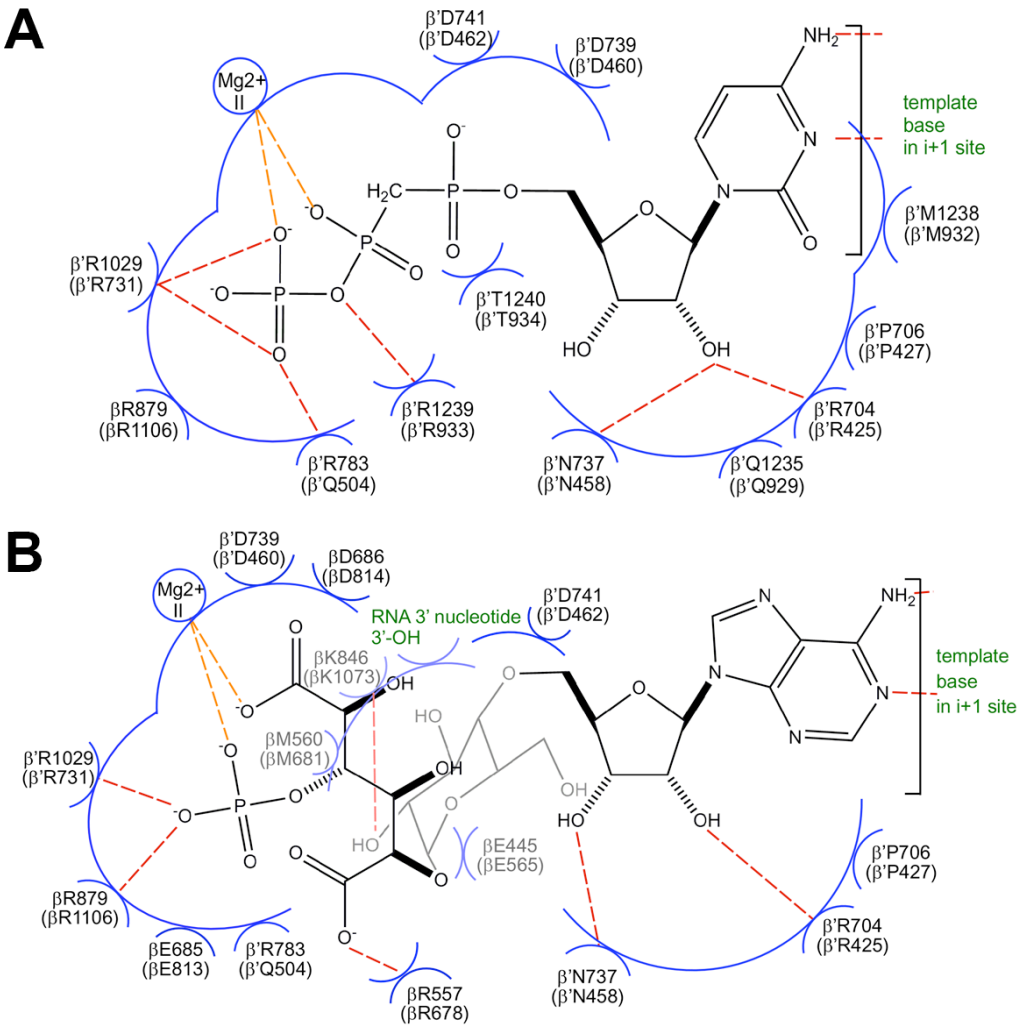


**Figure 14. Contacts between RNAP and CMPcPP/Thg (schematic)**

(A) Schematic summary of contacts of CMPcPP with RNAP residues and DNA template strand. RNAP residues are numbered as in *T.thermophilus* RNAP and *E.coli* RNAP in the parentheses. Red dashed lines, hydrogen bonds. Orange dashed lines, bonds coordinating $Mg^{2+}$. Blue arcs, van der Waals interactions.

(B) Schematic summary of contacts of Thg with RNAP residues, DNA template strand and RNA.

There are some subtle differences between the interactions of Thg with RPitc and that of CMPcPP with RPitc. While CMPcPP forms hydrogen bond with β'Arg783, Thg only has van der Waals interaction with it. The allaric acid moiety of Thg forms two more hydrogen bond with residues βArg557, βLys846 than CMPcPP does (Figure 13, Figure 14). Thg also has additional van der Waals interactions with residues βGlu445, βMet560, βGlu685 and βAsp686. (Figure 14).

The key interactions between Thg and RNAP involve RNAP residues that are conserved in bacterial RNAP and in eukaryotic RNAP I, II, and III, with the exception of residues βMet560 and β'Arg783 to which it has van der Waals interactions. All of the other residues mentioned above are conserved among bacterial and eukaryotic RNAP. This is consistent with the lack of selectivity of Thg for bacterial RNAP vs. eukaryotic RNAP I, II, and III.

In summary, the structure shows conclusively that Thg inhibits RNAP by functioning as an NAI which competes with ATP for binding to the RNAP active center "i+1" nucleotide binding site. Also, the structure provides valuable information for optimizing the inhibitor, Thg, and thus increase its binding affinity and potentially its selectivity between bacterial and eukaryotic RNAP.

## 4 Discussion

The crystal structure of RPo-GpA-Thg provides important implications for the development of selective NAIs of bacterial RNAP. Thg can be used at the starting point for antibacterial drug

discovery, specifically for NAI discoveries. Here we discuss and propose some potential methods to increase the affinity and specificity of Thg in order to develop a more desirable antibacterial drug.

### 4.1 Strategies to increase affinity

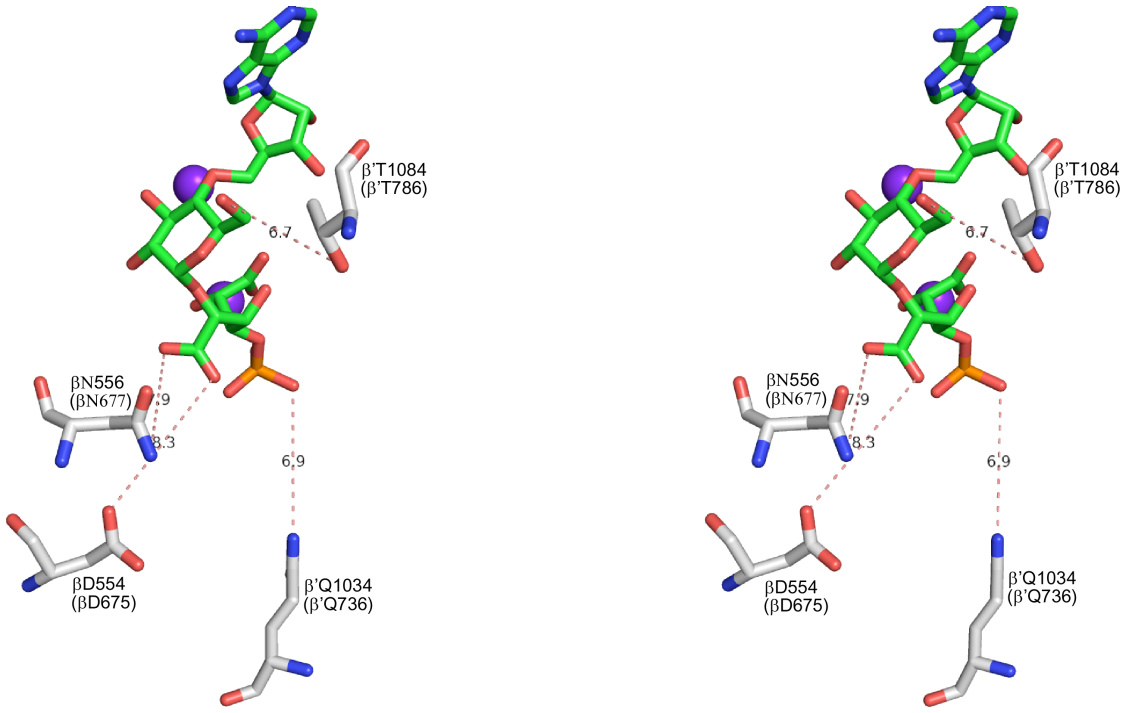


**Figure 15. Potential interactions for increasing affinity of Thg (stereodiagram)**

The residues that Thg that can be modified to interact with are shown in white sticks. Green sticks, Thg. Purple spheres, $Mg^{2+}$ (I) and $Mg^{2+}$ (II). The distances between Thg and the residues that Thg can be modified to potentially interact with are labeled. RNAP residues are numbered as in *T.thermophilus* RNAP and *E.coli* RNAP in the parentheses.

To increase the affinity for Thg with RNAP, we need to identify the sites on Thg that can be modified chemically and identify the amino acids within a reasonable distance that could

potentially interact with a modified Thg. There are 8 positions on Thg that could potentially be modified: the three hydroxyls of the glucose moiety, the two hydroxyls of the allaric acid moiety, the two hydroxyls on the two carboxyl groups of allaric acid moiety, and the hydroxyl on the phosphate moiety. We will not modify the adenosine moieties because it is important for base pairing at the "i+1" site. At the same time, we do not want to lose the exsisting important interactions such as coordination of $Mg^{2+}$ (II) , salt bridges between phosphate and arginine, etc.

As shown in Figure 15, the proposed strategies to increase affinity are: (1) modify the phosphate to be able to form a hydrogen bond with β'Gln1034 (current distance: 6.9 Å); (2) modify the carboxyl group of the allaric acid moiety to be able to form a salt bridge with βAsp554 (current distance: 8.3 Å) or to be able to form a hydrogen bond with βAsn556 (current distance: 7.9 Å); and (3) modify the hydroxyl of the glucose moiety shown in Figure 15 to be able to form a hydrogen bond with β'Thr1084 (current distance: 6.7 Å). For these modifications, the current position could be modified by forming an ester or amide and extending it with $(CH_2)_{2\sim4}$–OH or $(CH_2)_{2\sim4}$ $–NH_2$, such that the extended –OH and $–NH_2$ group can make interactions with the residues mentioned above.

### 4.2 Strategies to increase selectivity

Thg does not selectively inhibit bacterial RNAP, which is an important, unfavorable property which prevents it from being used as an antibacterial drug. In order to modify Thg so that it will

have selectivity for bacterial RNAP, we need to compare the structures of bacterial RNAP and eukaryotic RNAP at the active center "i+1" site, and identify potential changes to Thg that would increase its affinity for bacterial RNAP, while decreasing its affinity for eukaryotic RNAP. The structure of RPo-GpA-Thg is superimposed to the structure of *Saccharomyces cerevisiae* RNA Polymerase II Initiation Complex (PDB: 3ZRO) (Figure 16).

As shown in Figure 16, two potential modifications could be made to increase the selectivity of Thg. One would be to modify the carboxyl group hydroxyl of the allaric acid moiety of Thg, in order to extend the position with $-(CH_2)_{2\sim4}-NH_2$ so that it can form a salt bridge with βAsp554 (current distance: 8.3 Å). This would be expected to have only a weak interaction with the Gln763 of RPB2 subunit of *S. cerevisiae* RNAP at the same location. Another modification would be to modify the phosphate so that it can form a salt bridge with β'Glu734 (current distance: 10.6 Å), but would have only a weak interaction with the Ser476 of RPB1 subunit of *S. cerevisiae* RNAP at the same location. This modification, however, might be not too effective because the current distance is relatively far. In conclusion, the possible modifications for increasing the specificity of Thg are quite limited.

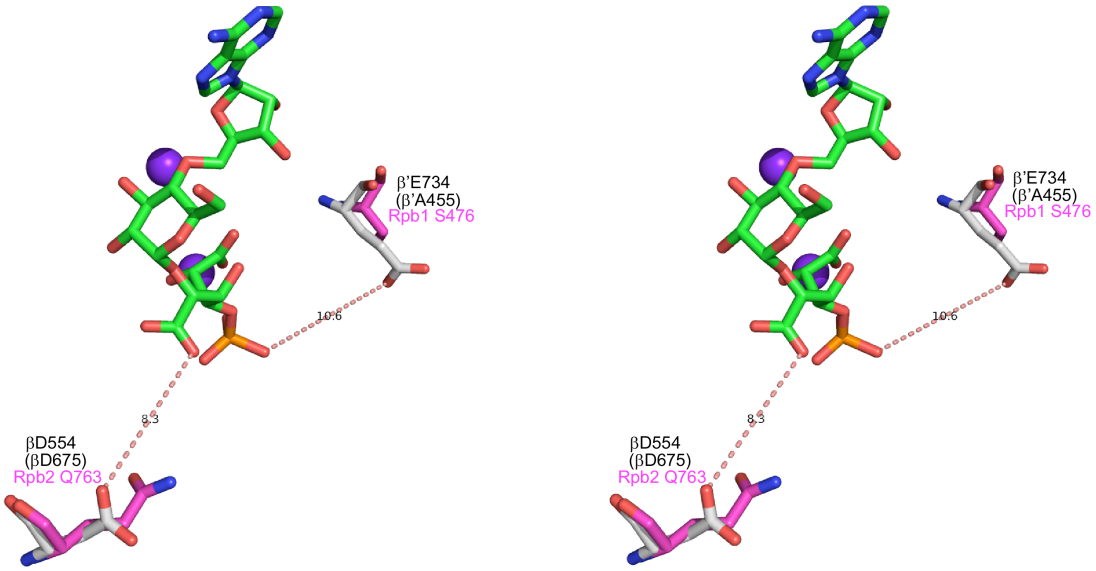


**Figure 16. Superimposition of *T.thermophilus* and *S. cerevisiae* RPitc at the "i+1" site (stereodiagram)**

The two residues that can be targeted for increasing selectivity are shown. *T.thermophilus* residues are shown as white sticks. *S. cerevisiae* residues are shown as magenta sticks. Thg is shown as green sticks. RNAP residues are labeled as in *T.thermophilus* RNAP, *E.coli* RNAP ( in the parentheses) and *S. cerevisiae* RNAP II (in magenta). Purple spheres, $Mg^{2+}$ (I) and $Mg^{2+}$ (II). The distance between Thg and the residues in *T.thermophilus* RNAP are

### 4.3 Thg-Sal bipartite inhibitor proposition

One way to dramatically increase both the affinity and selectivity of Thg at the same time is to develop a bipartite inhibitor that links salinamide with Thg.

Salinamide (Sal) is a previously identified bacterial RNAP inhibitor that inhibits RNAP by binding to the BH cap near the active center, and preventing the BH from undergoing conformational changes which are important for nucleotide addition (Degen et al., 2014). Sal is

selective for bacterial RNAP and does not inhibit eukaryotic RNAP (Degen et al., 2014). Furthermore, by superimposing the structure of *E.coli* RNAP-Sal (PDB: 4MEX) and *T.thermophilus* RPo-GpA-Thg (Figure 17), we find that the Thg binding site is very close to the Sal binding site. The distance between the carboxyl group hydroxyl of the Thg allaric acid moiety, and the epoxide moiety of Sal (the only easily modifiable position of Sal) (Figure 17) is only 4.3 Å in the superimposed structure. The distance between the phosphate hydroxyl of Thg and the epoxide moiety of Sal is 7.2 Å. This provides a feasible structure model for linking Thg and Sal together to form a bipartite inhibitor.

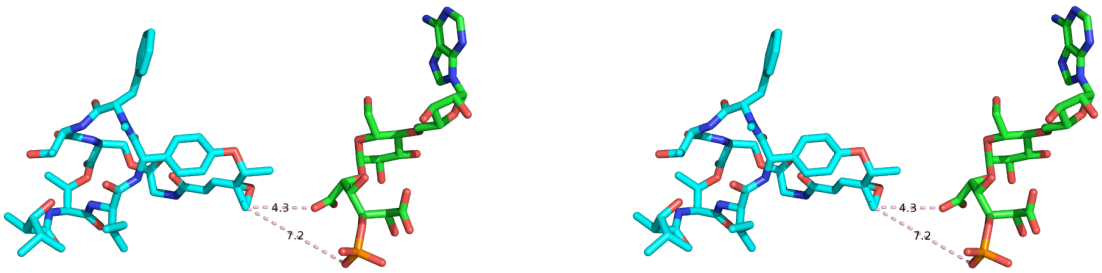


**Figure 17. Superimposition of structures of *E.coli* RNAP-Sal and *T.thermophilus* RPo-GpA-Thg (sterodiagram)**

Blue sticks: Sal A in the superimposed structure of *E.coli* RNAP-Sal on RPo-GpA-Thg. Green sticks: Thg in the structure of RPo-GpA-Thg. Distances between modifiable positions are labeled.

A bipartite inhibitor would be expected to have more potent activity against the enzyme than each of its two components individually because of its increased binding affinity for the enzyme (Brotz-Oesterhelt and Brunner, 2008). More importantly, since Sal can selectively bind to

bacterial RNAP, the proposed Thg-Sal bipartite inhibitor would overcome the non-selective property of Thg. This would make for a much more desirable antibacterial inhibitor.

## 5 Conclusions

In this thesis, we studied the structural basis for transcription inhibition of bacterial RNAP by the NAI, Thg. The structure shows that Thg binds to the RNAP active-center "i+1 site" in a way that resembles ATP binding at the "i+1 site," and, thus, Thg inhibits nucleotide addition. The structure defines the interactions between Thg and the RNAP "i+1 site," and suggests potential modifications to Thg and other nucleoside-analog inhibitors that could increase the affinity and selectivity of NAI inhibitors targeting the RNAP "i+1 site".

The binding site of Thg, the RNAP "i+1 site", is different from those of all other RNAP inhibitors that have been defined so far. This binding site is in the active center of the enzyme which contains many important structural and functional modules necessary for the enzymatic activity of RNAP. As a result mutations happen rarely in this region, and thus, the resistance rate to NAI inhibitors is expected to be significantly lower than that of other non-active-center-targeted inhibitors. Moreover, the development of a Thg-Sal bipartite inhibitor would further decrease the resistance rate. To become resistant to the bipartite inhibitor, the bacteria would have to develop mutations in both of the Thg target and the Sal target.

This structure of RNAP in complex with the non-selective NAI Thg is the first reported structure of a bacterial RNAP in complex with an NAI. NAIs of viral nucleotide polymerases have been the subject of intense interest, and immense importance, for the development of anti-HIV and anti-HCV drugs. NAIs of bacterial RNAP only now are beginning to be explored, but show high promise for the development of antibacterial drugs. The structures of the RNAP-Thg complexes provide a starting point for a structure-based understanding of the bacterial RNAP selectivity of NAIs, and for the structure-based design of more potent bacterial-RNAP-selective NAIs.

## Bibliography


1. Adams, P.D., Afonine, P.V., Bunkoczi, G., Chen, V.B., Davis, I.W., Echols, N., Headd, J.J., Hung, L.W., Kapral, G.J., Grosse-Kunstleve, R.W.*, et al.* (2010). PHENIX: a comprehensive Python-based system for macromolecular structure solution. Acta Crystallogr D Biol Crystallogr *66*, 213-221.
2. Artsimovitch, I., Chu, C., Lynch, A.S., and Landick, R. (2003). A new class of bacterial RNA polymerase inhibitor affects nucleotide addition. Science *302*, 650-654.
3. Brotz-Oesterhelt, H., and Brunner, N.A. (2008). How many modes of action should an antibiotic have? Curr Opin Pharmacol *8*, 564-573.
4. Burgess, R.R., Travers, A.A., Dunn, J.J., and Bautz, E.K. (1969). Factor stimulating transcription by RNA polymerase. Nature *221*, 43-46.
5. Campbell, E.A., Pavlova, O., Zenkin, N., Leon, F., Irschik, H., Jansen, R., Severinov, K., and Darst, S.A. (2005). Structural, functional, and genetic analysis of sorangicin inhibition of bacterial RNA polymerase. Embo J *24*, 674-682.
6. Chopra, I. (2007). Bacterial RNA polymerase: a promising target for the discovery of new antimicrobial agents. Curr Opin Investig Drugs *8*, 600-607.
7. Ciciliato, I., Corti, E., Sarubbi, E., Stefanelli, S., Gastaldo, L., Montanini, N., Kurz, M., Losi, D., Marinelli, F., and Selva, E. (2004). Antibiotics GE23077, novel inhibitors of bacterial RNA polymerase. I. Taxonomy, isolation and characterization. J Antibiot (Tokyo) *57*, 210-217.
8. Da, L.T., Pardo Avila, F., Wang, D., and Huang, X. (2013). A two-state model for the dynamics of the pyrophosphate ion release in bacterial RNA polymerase. PLoS Comput Biol *9*, e1003020.
9. Degen, D., Feng, Y., Zhang, Y., Ebright, K.Y., Ebright, Y.W., Gigliotti, M., Vahedian-Movahed, H., Mandal, S., Talaue, M., Connell, N.*, et al.* (2014). Transcription inhibition by the depsipeptide antibiotic salinamide A. Elife *3*, e02451.
10. deHaseth, P.L., Zupancic, M.L., and Record, M.T., Jr. (1998). RNA polymerase-promoter interactions: the comings and goings of RNA polymerase. J Bacteriol *180*, 3019-3025.
11. Emsley, P., Lohkamp, B., Scott, W.G., and Cowtan, K. (2010). Features and development of Coot. Acta Crystallogr D Biol Crystallogr *66*, 486-501.
12. Farkas, J., Sebesta, K., Horska, K., Samek, Z., Dolejs, L., and Sorm, F. (1969). Coll Czech Chem Commun, Eng Edn *34*, 1118-1120.
13. Ho, M.X., Hudson, B.P., Das, K., Arnold, E., and Ebright, R.H. (2009). Structures of RNA polymerase-antibiotic complexes. Curr Opin Struct Biol *19*, 715-723.
14. Kapanidis, A.N., Margeat, E., Ho, S.O., Kortkhonjia, E., Weiss, S., and Ebright, R.H.

(2006). Initial transcription by RNA polymerase proceeds through a DNA-scrunching mechanism. Science *314*, 1144-1147.

15. Kireeva, M.L., Opron, K., Seibold, S.A., Domecq, C., Cukier, R.I., Coulombe, B., Kashlev, M., and Burton, Z.F. (2012). Molecular dynamics and mutational analysis of the catalytic and translocation cycle of RNA polymerase. BMC Biophys *5*, 11.
16. Liu, X., Ruan, L., Peng, D., Li, L., Sun, M., and Yu, Z. (2014). Thuringiensin: a thermostable secondary metabolite from Bacillus thuringiensis with insecticidal activity against a wide range of insects. Toxins *6*, 2229-2238.
17. Losick, R., Chamberlin, M., and Cold Spring Harbor Laboratory. (1976). RNA polymerase (Cold Spring Harbor, N.Y., Cold Spring Harbor Laboratory).
18. Minakhin, L., Bhagat, S., Brunning, A., Campbell, E.A., Darst, S.A., Ebright, R.H., and Severinov, K. (2001). Bacterial RNA polymerase subunit omega and eukaryotic RNA polymerase subunit RPB6 are sequence, structural, and functional homologs and promote RNA polymerase assembly. Proc Natl Acad Sci U S A *98*, 892-897.
19. Mukhopadhyay, J., Sineva, E., Knight, J., Levy, R.M., and Ebright, R.H. (2004). Antibacterial peptide microcin J25 inhibits transcription by binding within and obstructing the RNA polymerase secondary channel. Mol Cell *14*, 739-751.
20. Naryshkin, N., Revyakin, A., Kim, Y., Mekler, V., and Ebright, R.H. (2000). Structural organization of the RNA polymerase-promoter open complex. Cell *101*, 601-611.
21. Nudler, E. (2009). RNA polymerase active center: the molecular engine of transcription. Annu Rev Biochem *78*, 335-361.
22. Revyakin, A., Liu, C., Ebright, R.H., and Strick, T.R. (2006). Abortive initiation and productive initiation by RNA polymerase involve DNA scrunching. Science *314*, 1139-1143.
23. Saecker, R.M., Record, M.T., Jr., and Dehaseth, P.L. (2011). Mechanism of bacterial transcription initiation: RNA polymerase - promoter binding, isomerization to initiation-competent open complexes, and initiation of RNA synthesis. J Mol Biol *412*, 754-771.
24. Sebesta, K., and Horska, K. (1970). Mechanism of inhibition of DNA-dependent RNA polymerase by exotoxin of Bacillus thuringiensis. Biochim Biophys Acta *209*, 357-376.
25. Sebesta, K., Horska, K., and Vankova, J. (1969). Coll Czech Chem Commun, Eng Edn *34*, 1786-1791.
26. Seibold, S.A., Singh, B.N., Zhang, C., Kireeva, M., Domecq, C., Bouchard, A., Nazione, A.M., Feig, M., Cukier, R.I., Coulombe, B.*, et al.* (2010). Conformational coupling, bridge helix dynamics and active site dehydration in catalysis by RNA polymerase. Biochimica et biophysica acta *1799*, 575-587.
27. Sosunov, V., Sosunova, E., Mustaev, A., Bass, I., Nikiforov, V., and Goldfarb, A. (2003). Unified two-metal mechanism of RNA synthesis and degradation by RNA polymerase. Embo J *22*, 2234-2244.
28. Srivastava, A., Talaue, M., Liu, S., Degen, D., Ebright, R.Y., Sineva, E., Chakraborty, A.,

Druzhinin, S.Y., Chatterjee, S., Mukhopadhyay, J.*, et al.* (2011). New target for inhibition of bacterial RNA polymerase: 'switch region'. Curr Opin Microbiol *14*, 532-543.

29. Vagin, A., and Teplyakov, A. (1997). MOLREP: an automated program for molecular replacement. J Appl Crystallogr *30*, 1022-1025.
30. Vassylyev, D.G., Vassylyeva, M.N., Perederina, A., Tahirov, T.H., and Artsimovitch, I. (2007a). Structural basis for transcription elongation by bacterial RNA polymerase. Nature *448*, 157-162.
31. Vassylyev, D.G., Vassylyeva, M.N., Zhang, J., Palangat, M., Artsimovitch, I., and Landick, R. (2007b). Structural basis for substrate loading in bacterial RNA polymerase. Nature *448*, 163-168.
32. Vassylyeva, M.N., Lee, J., Sekine, S.I., Laptenko, O., Kuramitsu, S., Shibata, T., Inoue, Y., Borukhov, S., Vassylyev, D.G., and Yokoyama, S. (2002). Purification, crystallization and initial crystallographic analysis of RNA polymerase holoenzyme from Thermus thermophilus. Acta Crystallogr D Biol Crystallogr *58*, 1497-1500.
33. Ventola, C.L. (2015). The antibiotic resistance crisis: part 1: causes and threats. P T *40*, 277-283.
34. Zhang, G., Campbell, E.A., Minakhin, L., Richter, C., Severinov, K., and Darst, S.A. (1999). Crystal structure of Thermus aquaticus core RNA polymerase at 3.3 A resolution. Cell *98*, 811-824.
35. Zhang, Y., Degen, D., Ho, M.X., Sineva, E., Ebright, K.Y., Ebright, Y.W., Mekler, V., Vahedian-Movahed, H., Feng, Y., Yin, R.*, et al.* (2014). GE23077 binds to the RNA polymerase 'i' and 'i+1' sites and prevents the binding of initiating nucleotides. Elife *3*, e02450.
36. Zhang, Y., Feng, Y., Chatterjee, S., Tuske, S., Ho, M.X., Arnold, E., and Ebright, R.H. (2012). Structural basis of transcription initiation. Science *338*, 1076-1080.